Hydrogen Permeation of Multi-Layered-Coatings

Motonori Tamura

University of Electro-Communications, Tokyo, Japan

tamura@uec.ac.jp

Keywords: Hydrogen permeation, microstructure, hydrogen traps, multi-layered-coatings.

Abstract. Using a substrate of AISI 316L austenitic stainless steel, which is used for components in high-pressure hydrogen systems, the hydrogen barrier properties of samples with single-layer coatings of TiC, TiN, and TiAlN as well as a multi-layered coating of TiAlN and TiMoN were evaluated. The ion plating method was used, and coating thicknesses of 2.0–2.6 μm were obtained. Hydrogen permeation tests were carried out under a differential hydrogen pressure of 400 kPa and at a temperature between 573 and 773 K, and the quantities of hydrogen that permeated the samples were measured. This study aimed at elucidating the relationship between the microstructures of the coatings and the hydrogen permeation properties. Coatings of TiC, TiN, TiAlN, and TiAlN/TiMoN facilitated reductions of the hydrogen permeabilities to 1/100 or less of that of the uncoated substrate. The samples coated with TiN and TiC that developed columnar crystals vertical to the substrate exhibited higher hydrogen permeabilities. The experiment confirmed that the coatings composed of fine crystal grains were highly effective as hydrogen barriers, and that this barrier property became even more efficient if multiple layers of the coatings were applied. The crystal grain boundaries of the coating and interfaces of each film in a multi-layered coating may serve as hydrogen trapping sites. We speculate that fine crystal structures with multiple crystal grain boundaries and multi-layered coating interfaces will contribute to the development of hydrogen barriers.

1. Introduction

The use of hydrogen fuel is a promising approach for reducing emissions of greenhouse gases. The hydrogen used in hydrogen fuel cells is an ideal energy source that only emits water and produces no greenhouse gases. However, to realize a hydrogen-energy-driven society, it is necessary to solve various technical issues resulting from the impact of hydrogen on the properties of various materials.

Hydrogen in many metallic materials, such as carbon steel [1-5], stainless steel [6-9], and aluminum alloys [10-12], affects their mechanical properties negatively. Steels mainly composed of high-strength ferrite and martensite structures have exceptionally high hydrogen diffusibilities and often exhibit hydrogen embrittlement [1-3]. In recent years, there have been many attempts to replace fossil fuels with hydrogen gas, and many hydrogen energy systems that use high-pressure hydrogen are being developed. AISI 316L austenitic stainless steels are known to have high durabilities and high resiliencies to environmental hydrogen embrittlement [13-16]. Their widespread industrial application demands not only the clarification of the interactions between high-pressure hydrogen and relevant materials but also the development of technology that prevents the penetration of hydrogen into these materials. Previous studies have shown that when steel is exposed to a hydrogen gas atmosphere, the hydrogen on the surface is relatively easily dissociated from a molecular state to an atomic state, penetrating the material and causing hydrogen embrittlement [4, 5].

Engineers and researchers of various systems, including fusion reactors, fuel cells, H_2S-corrosion resistant components, and vacuum devices, have developed barrier films that prevent hydrogen penetration of the material [17-22]. According to numerous reports, dense ceramic coatings of Al_2O_3, TiC, TiN, or BN can serve as efficient hydrogen barriers. There are many coating methods, including chemical vapor deposition, physical vapor deposition, and plasma sprays. Irrespective of the method, a ceramic coating of only a few micrometers can reduce the penetration of hydrogen by a few orders of magnitude. However, the reported hydrogen permeation reduction factors vary significantly. For example, for an Al_2O_3 coating, reported values for this factor range from 10 to 10,000.

Thin alumina deposited on amorphous tungsten oxide by a filtered vacuum arc method can reduce hydrogen permeation by a factor greater than 3,000, even for only thicknesses of 500 nm. However, plasma-sprayed coatings of alumina on steels are not very effective permeation barriers since the films contain many defects [20, 22].

These differences can be accounted for by the microstructures of the coating, which differ considerably depending on how they are formed, thereby influencing the hydrogen permeation behavior. Many engineers and researchers have reported these formation-condition-dependent differences in the microstructures, and some have modeled the most common microstructures [23-26]. The Thornton structure zone model, for example, classifies the microstructures based on the substrate temperature and argon pressure when the film is formed [23, 24]. With sputtering, a fine nano-structure and micrometer-sized columnar crystal grain structure can be formed. It is not known whether these microstructures exhibit the same hydrogen permeation behaviors.

In this research, the influence of the differences in the microstructures of various coatings on the hydrogen permeation behavior was studied, and the correlations between the influencing factors were analyzed.

2. Experimental Details

2.1. Characterization of coatings

Coatings were formed using the arc ion plating method. AISI 316L austenitic stainless steel was used as the substrate, and samples were laminated with each type of coating. The substrate was set in the film deposition device, evacuated, and its surface was subjected to ion bombardment treatment in an argon atmosphere. The substrate temperatures were 573–773 K. The reaction gases were C_2H_2 and N_2, maintained at pressures of 7–8 Pa. The substrate bias voltage was -135 V. Different coating microstructures were obtained by changing the substrate temperature and pressures of the reaction gases.

The arc ion plating method is a film-coating technology that uses a vacuum arc discharge between the target (coating film material) as the cathode, and an anode, thereby evaporating and ionizing a target material and subsequently depositing it on the surface of a substrate (object to be coated), to which a negative bias voltage is applied. This method provides a high ionization ratio of the evaporated materials. This method enables the deposition of a film with a high density and good adhesion strength. The coatings deposited by this method are commonly used for cutting tools, and representative coatings include TiAlN coatings.

Multiple evaporation sources with a plate target are equipped on the lateral side of a vacuum chamber, and a substrate table is set in the chamber. The multiple evaporation sources are typically arrayed in the vertical direction to ensure film thickness uniformity in the vertical direction and to provide a wide coating area. The table is rotated by a rotating mechanism so that a large quantity of substrates can be coated uniformly along the circumference.

In recent years, hard coatings for cutting tools have become necessary to achieve high wear resistance performances under extremely severe environments. Typically, these improvements have been achieved by multiple element additions and multilayered structures. The coatings deposited by this method have unique structures in which hard layers are combined with functional layers, or the stacking period of the layers is adjusted to achieve a variety of characteristics. Single-layered

coatings of TiC, TiN, and TiAlN and a multi-layered coating of TiAlN/TiMoN were applied. The thicknesses of the coatings ranged between 2.0 and 2.6 μm.

Crystal phase analyses of the coatings were carried out using X-ray diffraction and electron-beam diffraction. The thicknesses of the coating cross-sections were measured and the microstructures were observed via scanning electron microscopy. The coating surface roughness and crystal grain analyses were carried out using scanning probe microscopy (SPM). Crystal grain size measurements and crystal phase analysis inside the coatings, via coating cross-sectional analysis, were conducted using transmission electron microscopy (TEM).

Using SPM, the sample surfaces in the atmosphere can be easily measured at high resolutions [27-30]. The properties of the coating surface can be analyzed using image analysis software. A method that binarizes the unevenness of the surface and generates an image can be applied to better understand the crystal grains of the coating. From a crystal cross-section in a plane parallel to the substrate surface (coating surface), the average value for the crystal grain size can be calculated by assuming that the crystals are spherical [27, 28]. In this study, the crystal grain size measurements were performed by a coating cross-sectional analysis using TEM, as this provided high-accuracy results. The diameters of 20 crystals taken from five arbitrary cross-sections in a plane parallel to the substrate surface were determined from a TEM image, and an average diameter of these 20 crystals was calculated.

2.2. Hydrogen permeation tests

Hydrogen permeation tests were conducted with the differential pressure method stipulated in ISO 15105-1 [31-33]. A disk of AISI 316L austenitic stainless steel with a diameter of 30 mm and thickness of 0.1 mm was used as the substrate of the sample.

A hydrogen pressure of 400 kPa was applied to the coated surface of the sample, and the hydrogen was evacuated from the opposite side of the sample. Following a previous study [17], the hydrogen permeation behavior and mechanism can be categorized in the “diffusion-limited regime” between 100 and 800 kPa.

The amount of hydrogen that permeated the sample was quantitatively measured by gas chromatography. The sample was maintained with a susceptor made of silicone fiberglass. This was maintained at the test temperature under a vacuum, and hydrogen pressure was applied to its coated side. A measurement began when the quantity of hydrogen that permeated the sample reached a constant level. A metallic gold seal, with a low hydrogen reaction rate and high shielding properties against gas, was used as the material to maintain the sample. Three test temperatures of 573, 673, and 773 K were used. Under these test conditions, the hydrogen permeation of a coated sample is limited by the speed of hydrogen diffusion in the coating [25, 31-33]. The sample was maintained at the test temperature, and the hydrogen permeation began. The hydrogen permeation became constant after three hours, and thus, this measured value was defined as the hydrogen permeability.

As shown in Figure 1, the hydrogen permeability Φ can be calculated from the hydrogen permeation J, thickness of the sample ($d_{film} + d_{substrate}$), hydrogen permeation area A, and hydrogen differential pressure ($P^{1/2}_{,H2in} - P^{1/2}_{, H2out}$).

3. Results and discussion

3.1. Hydrogen permeation behavior

Figure 1 summarizes the hydrogen permeation behaviors of the samples prepared in this study. The TiC, TiN, TiAlN, and multi-layered TiAlN/TiMoN coatings were dense and exhibited excellent adhesion to the AISI 316L austenitic stainless steel substrate.

The hydrogen permeability of all the coated samples decreased compared with that of the substrate alone, confirming the effectiveness of the coatings as hydrogen barriers.

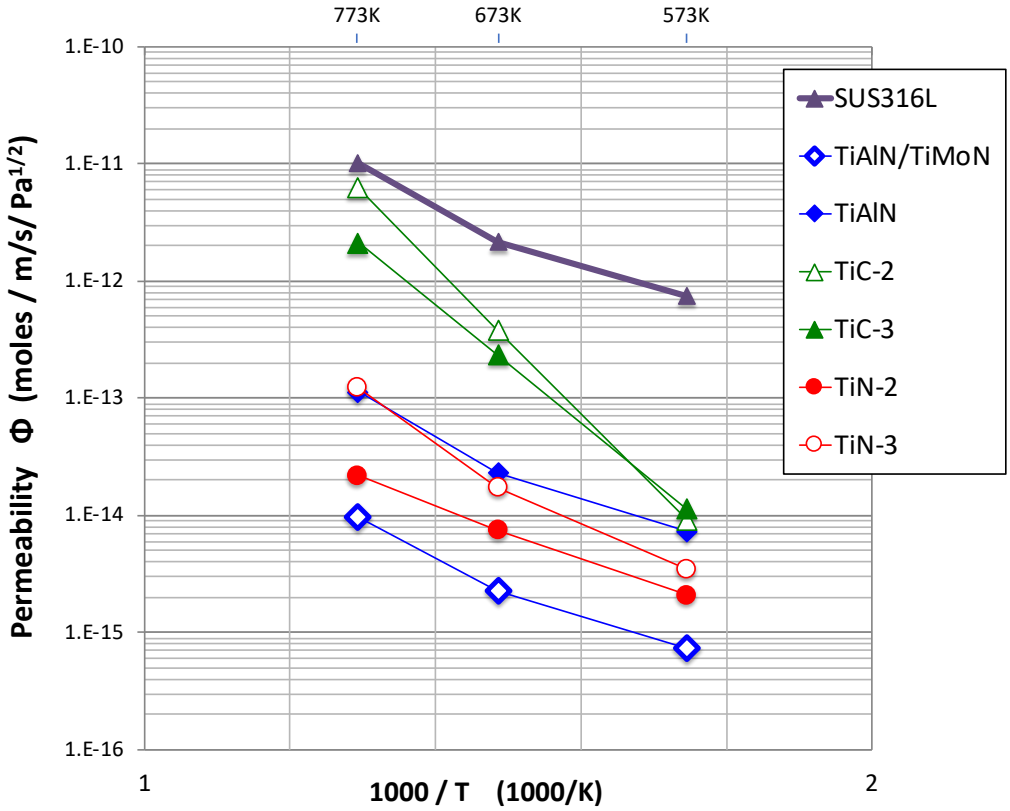

Figure 1. Hydrogen permeability of coated samples as a function of temperature.

A comparison of the results obtained at a test temperature of 573 K showed that the hydrogen permeabilities of the TiAlN-coated, TiN-coated, and TiAlN/TiMoN multi-layered coating samples were 1/100, 1/100 or less, and 1/1,000 of that of the uncoated substrate, respectively.

The hydrogen permeability varied greatly with the test temperature, with greater variations at lower temperatures. This permeability, shown in Figure 1, can reflect the hydrogen diffusion in the coating.

The implication is that in these hard coatings, lower temperatures result in lower diffusion coefficients of hydrogen. In other words, the highly sloped lines of the hydrogen permeability of each sample versus temperature indicate that the hydrogen diffusion activation energies are large

3.2. Effect of the microstructures of coatings on hydrogen permeation behavior

The relationship between the crystal grain size of the TiN-coated sample and hydrogen permeability is shown in Figure 2. Coating samples with small crystal grain sizes exhibited low hydrogen permeabilities.

Based on the TEM cross-section structure results, the correlation between the fine crystal structure of the coating and the hydrogen permeation behavior was examined in more detail.

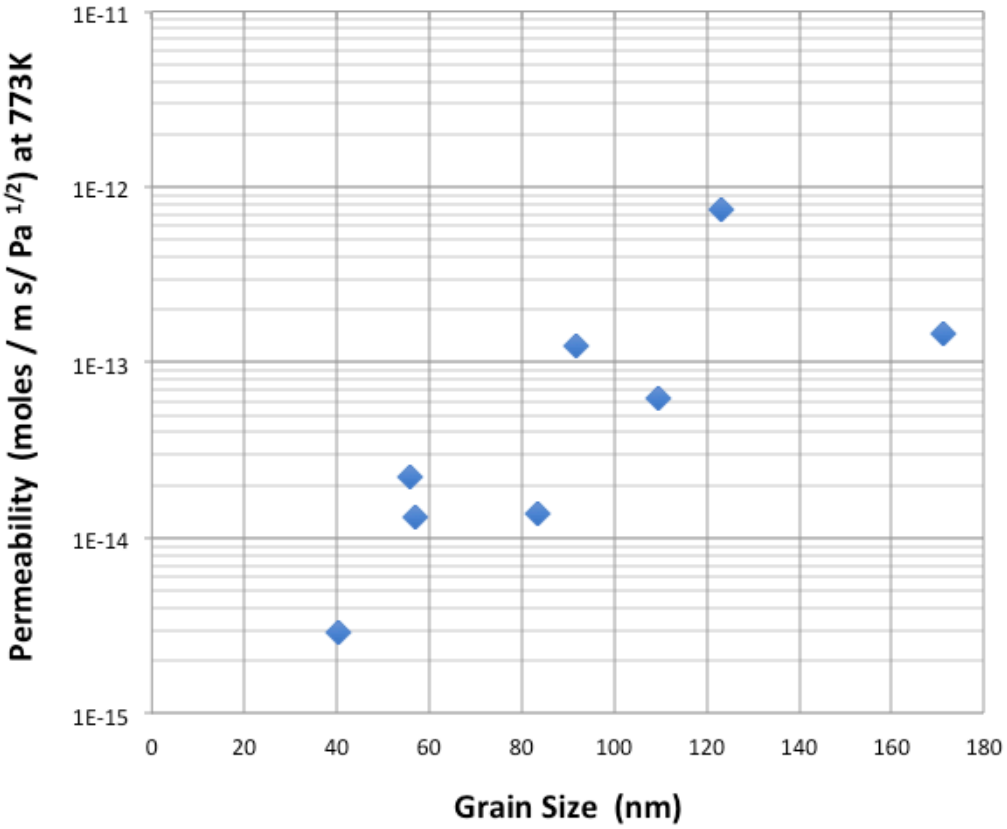

Figure 2. Hydrogen permeability of TiN-coated samples as a function of grain size.

Sample TiC-3 is composed of fine crystal grains with an average size of around 69 nm and corresponds to Zone T (transition structure, densely packed fibrous grains) of Thornton's structure zone model [23, 24]. Conversely, sample TiC-2 showed a form that corresponds to the Zone II (columnar) structure of this model. The average crystal grain size of sample TiC-2 was around 98 nm. The hydrogen permeability of TiC-3, which had finer crystal grains, was lower.

Sample TiN-2 was composed of fine crystal grains with an average size of around 56 nm and corresponded to Zone T. In contrast, TiN-3 had an average crystal grain size of around 92 nm, and a form that corresponded to the Zone II (columnar) structure. The hydrogen permeability of TiN-2, which had fine crystal grains, was once again lower than that of TiN-3.

The results confirm that the coatings with fine crystal grains that correspond to Zone T were highly effective hydrogen barriers. The coatings with fine crystal grains had many crystal grain boundaries, and it was possible that when hydrogen passed through a crystal grain boundary, the boundary served as a barrier to diffusion.

Based on previous research of the forms of hydrogen found inside materials, examples of hydrogen trapping sites are lattice defects (atom vacancies, dislocation, and crystal grain boundaries), impurity atoms, precipitates, inclusion interfaces, and voids. At hydrogen trapping sites, the diffusion of hydrogen is limited. For a hydrogen atom to escape from a trap site and continue to diffuse, a certain amount of activation energy is necessary.

Hydrogen diffusion behaviors inside metal materials, especially the mechanism of hydrogen embrittlement of steel, have been studied extensively since the 1970's. The quantity limit and solid solubility of hydrogen inside a crystal lattice are determined from the hydrogen quantity of a pure iron sample in a high-purity hydrogen gas environment and equilibrium [1-4]. Solid solubility is the ratio of the number of hydrogen atoms to the number of normal lattice points, whereas the hydrogen concentration is proportional to the square root of the hydrogen gas pressure. Although the solid solubility of hydrogen in steel may be affected by the purity of the sample and surface conditions,

the results of various research studies performed at approximately 673 K or above concur that the temperature dependence is nearly a linear Arrhenius plot [1-5]. This is attributed to an essential phenomenon associated with the solid solution state, such as the inter-lattice position occupied by the hydrogen. Furthermore, the good data correlation for various samples indicates that the quantity of hydrogen that iron can absorb at 673 K or above is not strongly affected by lattice defects, such as impurities and crystal grain boundaries.

In contrast, it is known that with Ni, the hydrogen solid solubility varies considerably between single and multi-crystal samples [36]. Some studies emphasized that at temperatures of 573 K or lower, the solubility of iron alloys is also influenced by the surface adsorption reaction and lattice defects [5]. Other sources indicate that the hydrogen diffusion coefficient in steel is dependent on the crystal grain size [37]. That is, if the crystal grain size is small, the diffusion coefficient also decreases [36]. This suggests that when the diffusion speed of hydrogen is relatively low, the influence of crystal grain boundaries cannot be ignored.

The hydrogen diffusion coefficient in ionically or covalently bonded substances, such as ceramic coatings, is several times lower than that in steel [18, 19, 26], which suggests that the hydrogen trapping site effect works very efficiently. The fact that the crystal grains of the coating are fine suggests that these acted as barriers to the diffusion of hydrogen and contributed to improving the function of the coating.

In multi-layered coatings, as crystal grain boundaries become hydrogen diffusion barriers, the interfaces of the films may also become hydrogen diffusion barriers. Figure 3 shows the result of the TEM cross-section observation of the TiAlN/TiMoN multi-layered coating. It is possible to verify that many layers of a crystalline coating with thickness of around 5–10 nm were laminated onto a TiAlN single-layer coating (Figure 4). All these coatings were crystalline (Figures 5).

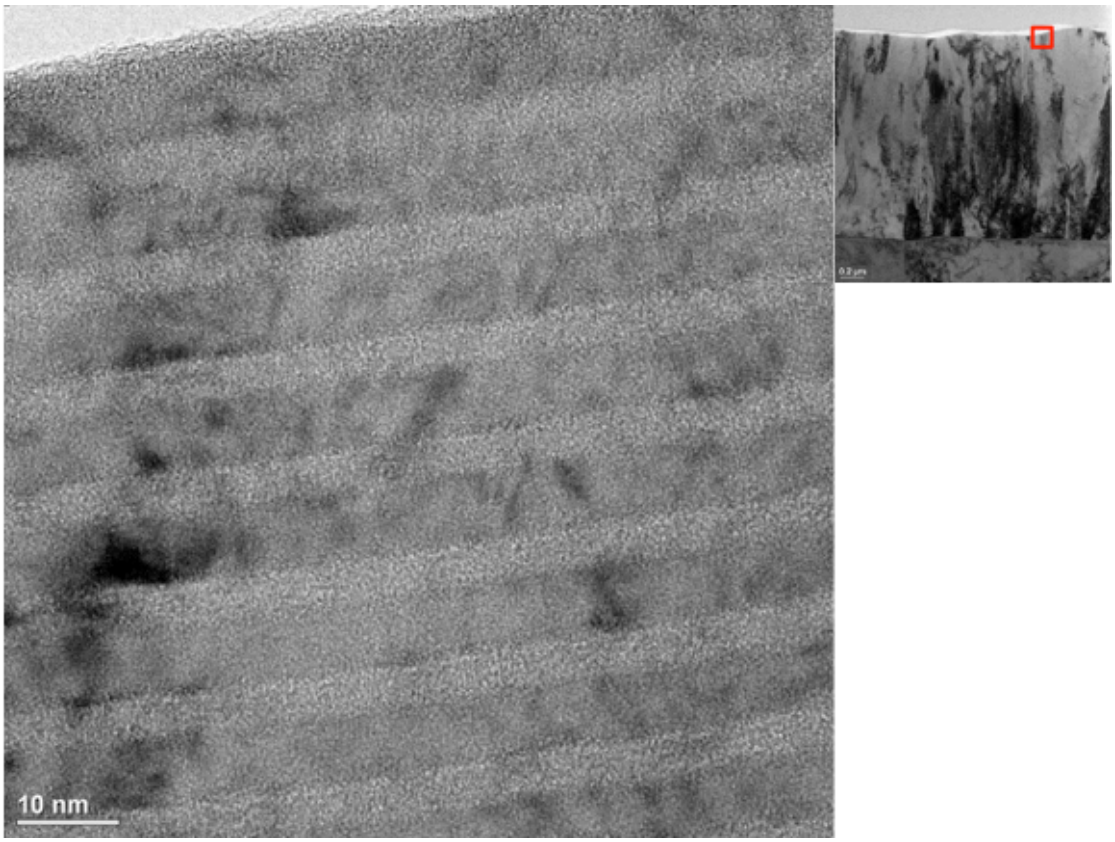

Figure 3. TEM image of cross section of the upper part of TiAlN/TiMoN multi-layer coating.

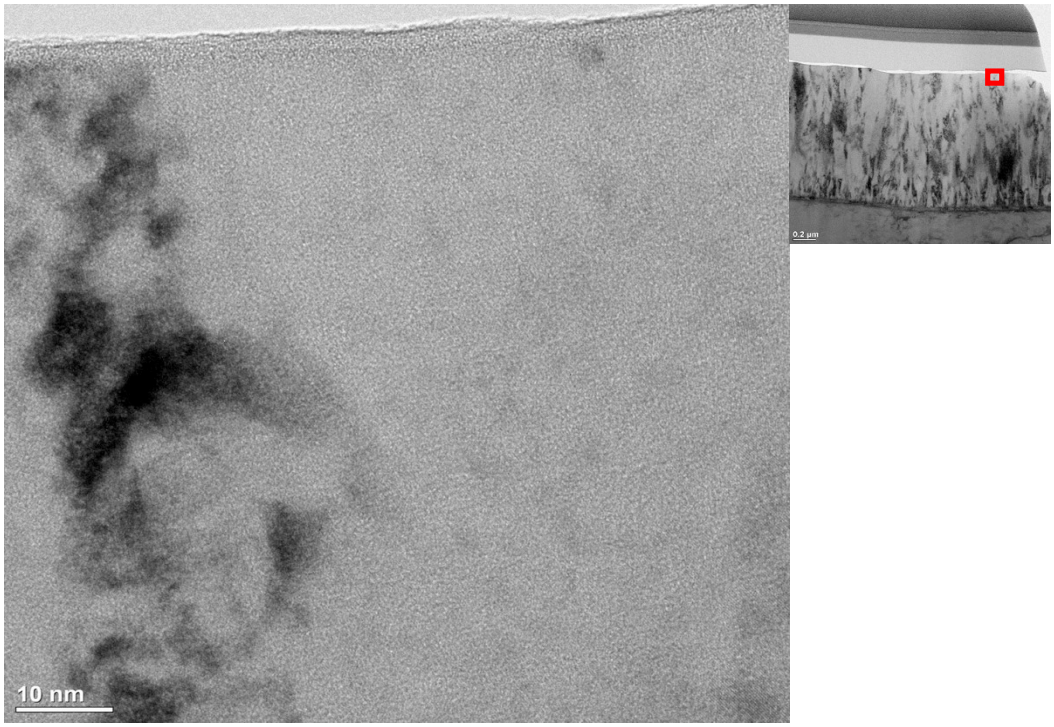

Figure 4. TEM image of cross section of the upper part of TiAlN coating.

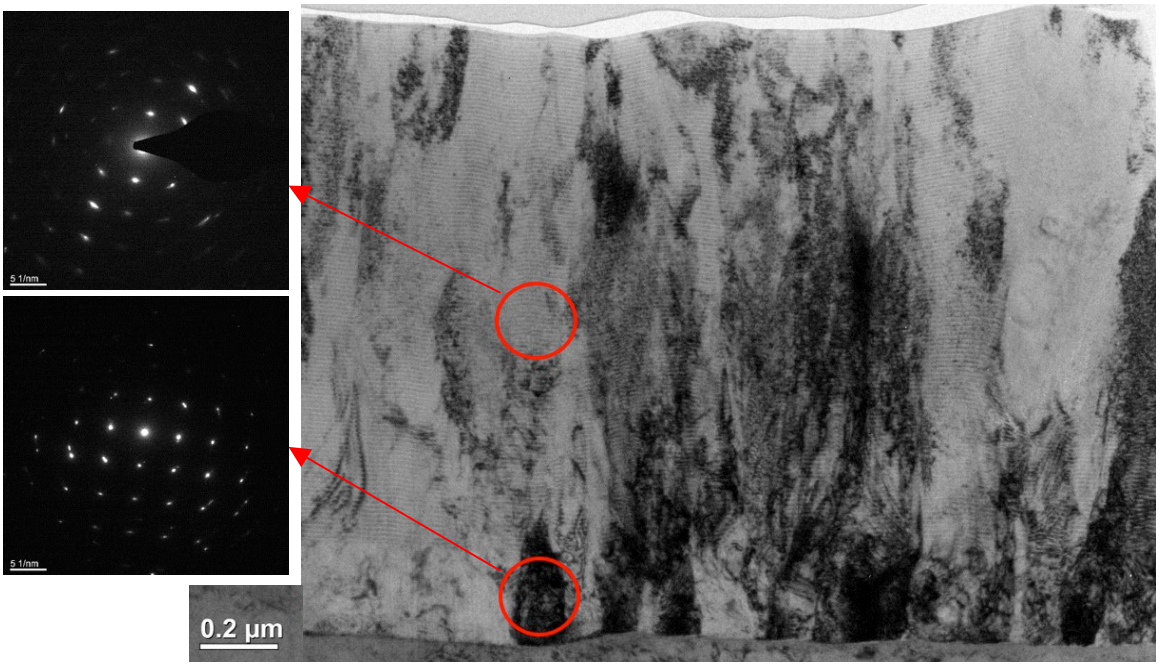

Figure 5. TEM image and diffraction pattern of TiAlN/TiMoN multi-layer coating.

As shown in Figure 1, the TiAlN/TiMoN multi-layered coating exhibited the lowest hydrogen permeability of all the coatings in this study, demonstrating that the interface effectively served as a hydrogen diffusion barrier.

Figure 6 shows a schematic diagram of the film interface serving as a hydrogen trap. The hydrogen atoms that diffuse into the coating can be trapped in the crystal grain boundaries and at the film interface.

Based on the findings above, we believe that in the fine crystal grain coating and the multi-layered coating, the crystal grain boundary and film interfaces serve as hydrogen diffusion barriers to reduce the hydrogen permeability, and that these hydrogen barrier coatings are more efficient when they possess these microstructures.

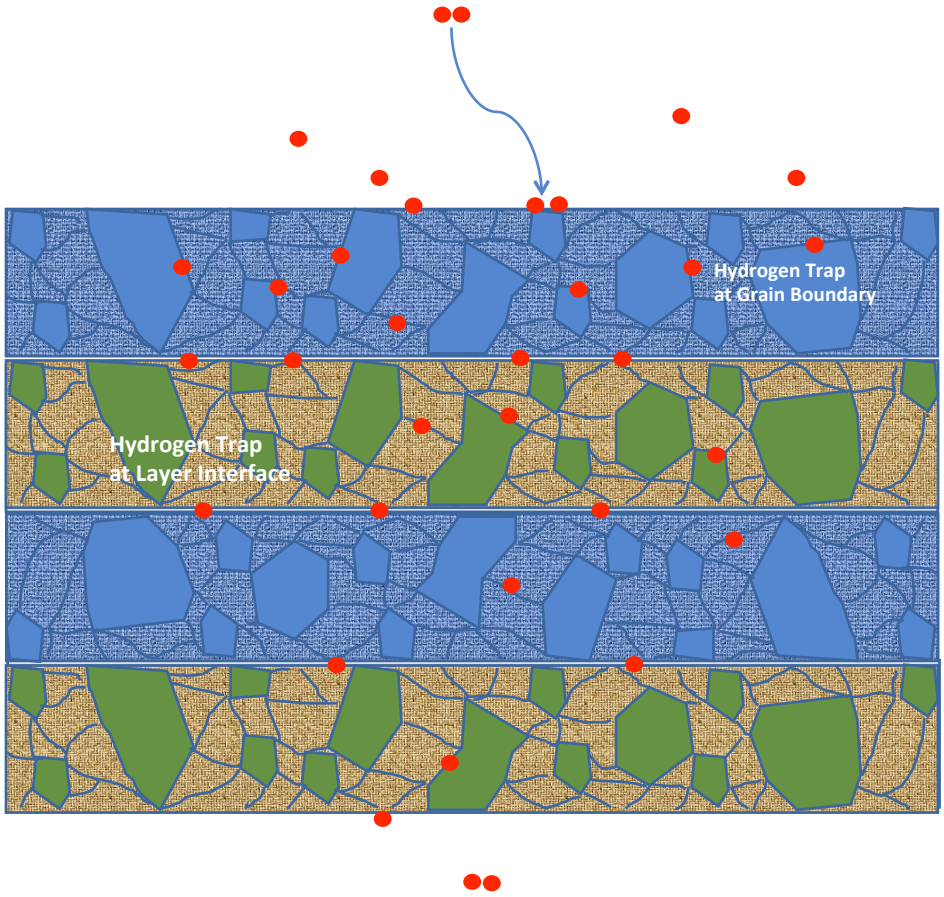

Figure 6. Schematic illustration of hydrogen traps at grain boundary and layer-interface. Hydrogen atoms can be trapped at grain boundary and layer-interface in coatings.

4. **Conclusions**

This study confirmed that coatings of TiC, TiN, and TiAlN and the multi-layered coating of TiAlN/TiMoN were dense and effectively served as hydrogen barriers.

When compared at a test temperature of 573 K, the hydrogen permeabilities of the TiAlN-coated, TiN-coated, and TiAlN/TiMoN multi-layered coating samples were 1/100, 1/100 or less, and 1/1,000 of that of the uncoated substrate, respectively.

The tests confirmed that coatings with fine crystal grains were highly efficient hydrogen barriers. It is speculated that these coatings possessed many crystal grain boundaries that served as barriers to the diffusion of hydrogen.

According to previous research on the forms of hydrogen inside materials, examples of hydrogen trap sites are lattice defects (atom vacancies, dislocation, and crystal grain boundaries), impurity atoms, precipitates, inclusion interfaces, and voids. However, which defects in the coatings affect the hydrogen barrier, as well as the extent of this influence, are subjects of future research. The diffusion movement of hydrogen is limited at hydrogen trapping sites.

It is speculated that the hydrogen atoms that diffuse into the coating are effectively trapped in the crystal grain boundaries and at the film interfaces. Among all the coatings tested, the TiAlN/TiMoN multi-layered coating exhibited the lowest hydrogen permeability.

The results of this study indicate that, in the fine crystal grain and the multi-layered coatings, the crystal grain boundaries and film interface served as hydrogen diffusion barriers to reduce the hydrogen permeability, and these hydrogen barrier coatings were more efficient when these microstructures were present. As such, we speculate that development of coating microstructures will become increasingly important for the development of hydrogen barrier coatings in the future.

References

[1] I. M. Robertson, P. Sofronis, A. Nagao, M. L. Martin, S. Wang, D. W. Gross, K. E. Nygren, Hydrogen embrittlement understood, Metall. Trans. A 46, (2015) 2323-2341.

[2] C. D. Beachem, A New Model for Hydrogen-Assisted Cracking (Hydrogen 'Embrittlement'), Metall. Trans. 3, (1972) 437-451.

[3] J. P. Hirth, Effects of Hydrogen on the Properties of Iron and Steel, Metall. Trans. A 11, (1980) 861-890.

[4] M. Nagumo, M. Nakamura, K. Takai, Hydrogen Thermal Desorption Relevant to Delayed-Fracture Susceptibility of High-Strength Steels, Metall. Trans. A 32, (2001) 339-347.

[5] K. Takai, Y. Homma, K. Izutsu, M. Nagumo, Identification of Trapping Sites in High-Strength Steels by Secondary Ion Mass Spectrometry for Thermal Desorbed Hydrogen, J. Jpn. Inst. Met. 60, (1996) 1155-1162.

[6] M. B. Whiteman, A. R. Troiano, Hydrogen Embrittlement of Austenitic Stainless Steels, Corrosion 21, (1965) 53-56.

[7] C. L. Briant, Hydrogen assisted cracking of type 304 stainless steel, Metall. Trans. A 10, (1979) 181-189.

[8] S. Fukuyama, K. Yokogawa, K. Kubo, M. Araki, Fatigue Properties of Type 304 Stainless Steel in High Pressure Hydrogen at Room Temperature, Trans. Jpn. Int. Met. 26, (1985) 325-331.

[9] G. Han, J. He, S. Fukuyama, K. Yokogawa, Effect of Strain-Induced Martensite on Hydrogen Environment Embrittlement of Sensitized Austenitic Stainless Steels at Low Temperature, Acta Mater. 46, (1998) 4559-4570.

[10] S. Osaki, D. Itoh, M. Nakai, SCC properties of 7050 series aluminum alloys in T6 and RRA tempers, J. JILM. 51 (2001) 222-227.

[11] M. Ando, M. Senoo, M. Kanno, Environmental embrittlement in air of Al–Zn–Mg–Cu alloys with Cr or Zr , J. Jpn. Inst. Light Met. 57, 19 (2007)19-24.

[12] G. A. Young Jr., J. R. Scully, The effects of test temperature, temper, and alloyed copper on the hydrogen-controlled crack growth rate of an Al-Zn-Mg-(Cu) alloy, Metall. Trans. A 33, 101 (2002) 101-115.

[13] C. San Marchi, B. P. Somerday, S. L. Robinson, Permeability, solubility and diffusivity of hydrogen isotopes in stainless steel, Int. J. Hydrogen Energy 32, (2007)100-116.

[14] S. K. Lee, H. S. Kim, S. J. Noh, Hydrogen Permeability, Diffusivity, and Solubility of SUS 316L Stainless Steel in the Temperature Range 400 to 800 ℃ for Fusion Reactor Applications, J. Korean Phys. Soc. 5, (2011) 3019-3023.

[15] K. Horikawa, H. Okada, H. Kobayashi, W. Urushihara, ydrogen Permeation Estimated by HMT in Carbon Steel Exposed to Gaseous Hydrogen, J. Jpn. Inst. Met 74, (2010) 199-204.

[16] M. Tamura, K. Shibata, Evaluation of Mechanical Properties of Metals at 45 MPa Hydrogen, J. Jpn. Inst. Met. 69, (2005) 1039-1048.

[17] M. Tamura, M. Noma, M. Yamashita, Characteristic Change of Hydrogen Permeation in Stainless Steel Plate by BN Coating, Surf. Coat. Technol. 260, (2014) 148-154.

[18] J. Yamabe, S. Matsuoka, Y. Murakami, Surface Coating with a High Resistance to Hydrogen Entry under High-Pressure Hydrogen-Gas Environment, Int. J. Hydrogen Energy 38, (2013) 10141-10154.

[19] M. Tamura, Hydrogen Permeation Characteristics of TiN-Coated Stainless Steels, J. Mat. Sci. Eng. A 5 (5-6) (2015) 197-201.

[20] R. G. Song, Hydrogen permeation resistance of plasma-sprayed Al2O3 and Al2O3–13wt.% TiO2 ceramic coatings on austenitic stainless steel, Surf. Coat. Technol. 168, 191 (2003) 191-194.

[21] T. Chikada, A. Suzuki, Z. Yao, D. Levchuk, H. Mainer, T. Terai, T. Muroga, Surface Behavior in Deuterium Permeation through Erbium Oxide Coating, Fusion Eng. Des. 84, (2009) 590-592.

[22] G. W. Hollenberg, E. P. Simonen, G. Kalinin, A. Terlain, Tritium/Hydrogen Barrier Development, Fusion Eng. Des. 28, (1995) 190-208.

[23] J. A. Thornton, Influence of Apparatus Geometry and Deposition Conditions on the Structure and Topography of Thick Sputtered Coatings, J. Vac. Sci. Technol. 11, (1974) 666-67-.

[24] J. A. Thornton, High Rate Thick Film Growth, Ann. Rev. Mater. Sci. 7, (1977) 239-260.

[25] J. W. Evans, P. A. Thiel. M. C. Bartelt, Morphological evolution during epitaxial thin film growth, Surf. Sci. Rep. 61, (2006) 1-128.

[26] J. L. Plawsky, A. G. Fedorov, S. V. Garimella, H. B. Ma, S. C. Maroo, L. Chen, Y. Nam, Nano- and Microstructures for Thin-Film Evaporation—A Review, Nanoscale and Microscale Themophys. Eng. 18, (2014) 251-269.

[27] D. A. Kiselev, I. K. Bdikin, E. K. Selezneva, K. Bormanis, A. Sternberg, A. L. Kholkin, Grain size effect and local disorder in polycrystalline relaxors via scanning probe microscopy, J. Phys. D: Appl. Phys. 40, (2007) 7109-7112.

[28] B. S. Lamsal, M. Dubey, V. Swaminathan, Y. Huh, D. Galipeau, Q. Qiao, Q. H. Fan, Nanoscale Investigation of Grain Growth in RF-Sputtered Indium Tin Oxide Thin Films by Scanning Probe Microscopy, J. Mater. 11, (2014) 3965-3972.

[29] P. Y. Huang, C. S. Ruiz-Vargas, A. M van der Zande, W. S. Whitney, M. P. Levendorf, J. W. Kevek, S. Garg, J. A. Alden, C. J. Hustedt, Y. Zhu, J. Park, P. L. McEuen, D. A. Muller, Grains and grain boundaries in single-layer graphene atomic patchwork quilts, Nature 469, (2011) 389-392.

[30] S. Choi, J. Heo, D. Kim, I. Chung, Ferroelectric properties of nano-size PZT grains determined by surface potential utilizing Kelvin force microscopy, Thin Solid Films 464-465, 277 (2004) 277-281.

[31] S. A. Stern, The “Barrer” Permeability Unit, J. Polym. Sci., Part A-2 6, (1968) 1933-1934.

[32] JIS K7126-2:2006 (Japanese Industrial Standards Committee).

[33] ISO15105-1:2007 (International Organization for Standardization).

[34] D. Gaude-Fugarolas, Proceedings of METAL, Effect of microstructure and trap typology on hydrogen redistribution in steel, Brno. Czech Repubulic, EC (2013) 15-17.

[35] R. Koyama, G. Itoh, Hydrogen emission at grain boundaries in tensile-deformed Al−9%Mg alloy by hydrogen microprint technique, Trans. Nonferrous Met. Soc. China 24, (2014) 2102-2106.

[36] A. Oudriss, J. Creus, J. Bouhattate, E. Conforto, C. Berziou, C. Savall, X. Feaugas, Grain Size and Grain-Boundary Effects on Diffusion and Trapping of Hydrogen in Pure Nickel, Acta Mater. 60, (2012) 6814-6828.

[37] N. Yazdipour, D. Dunne, E. Perelome, Effect of Grain Size on the Hydrogen Diffusion Process in Steel Using Cellular Automaton Approach, Mater. Sci. Forum 706-709, (2012) 1568-1573.